Figures

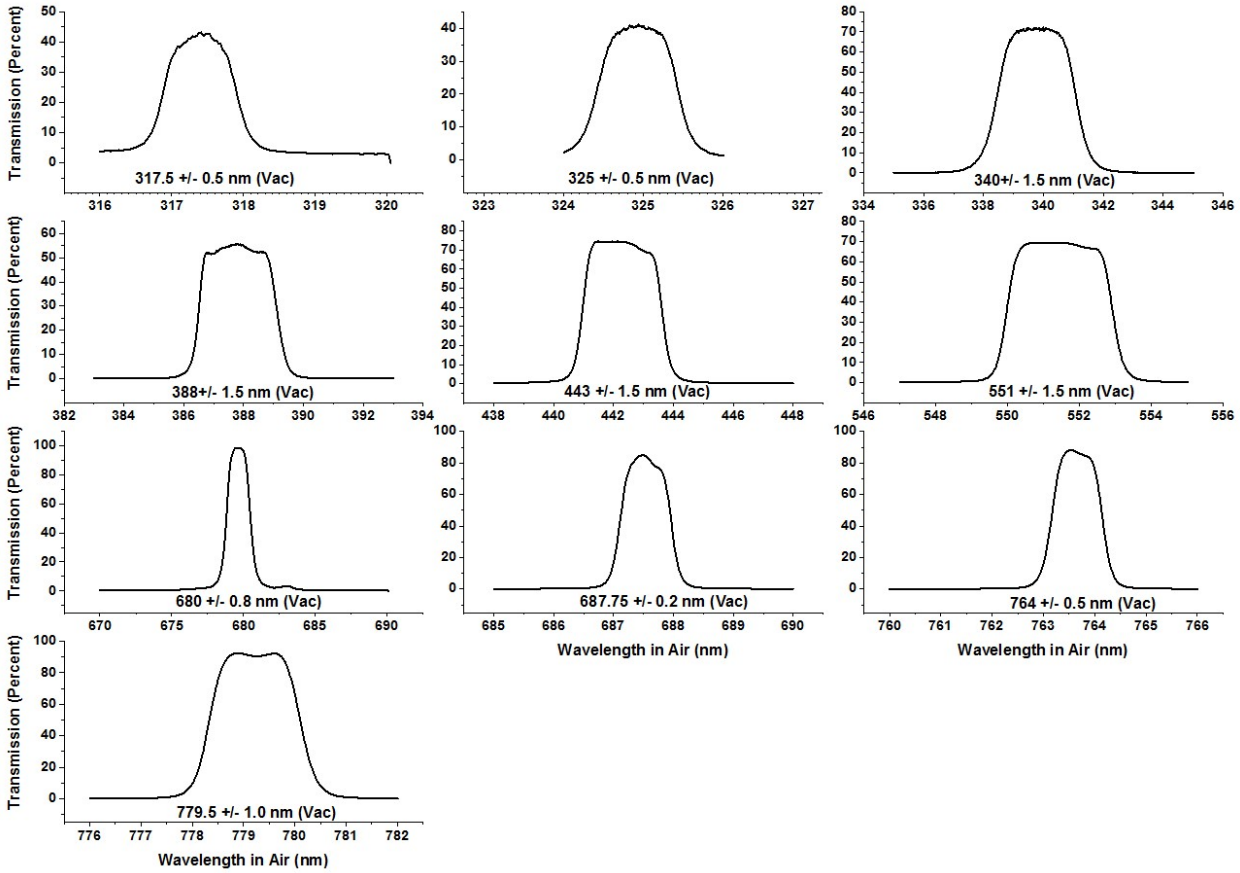

Figure 1-1 Filter transmission (percent) for the 10 EPIC wavelengths

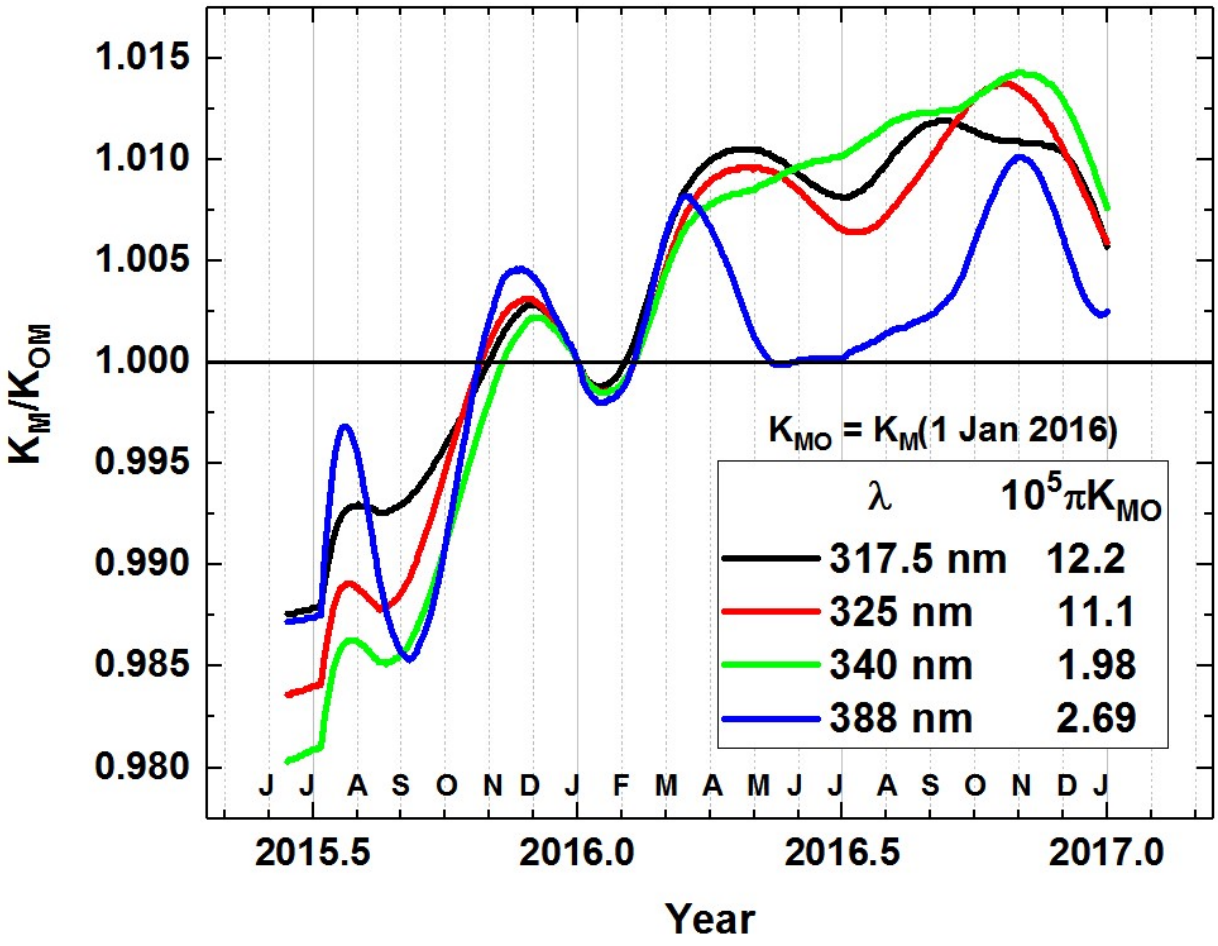

Figure 1-2 Normalized calibration function referenced to its value at 4 Jan 2016 when D_E = 1 au. Average rate of increase is 0.016 per year.

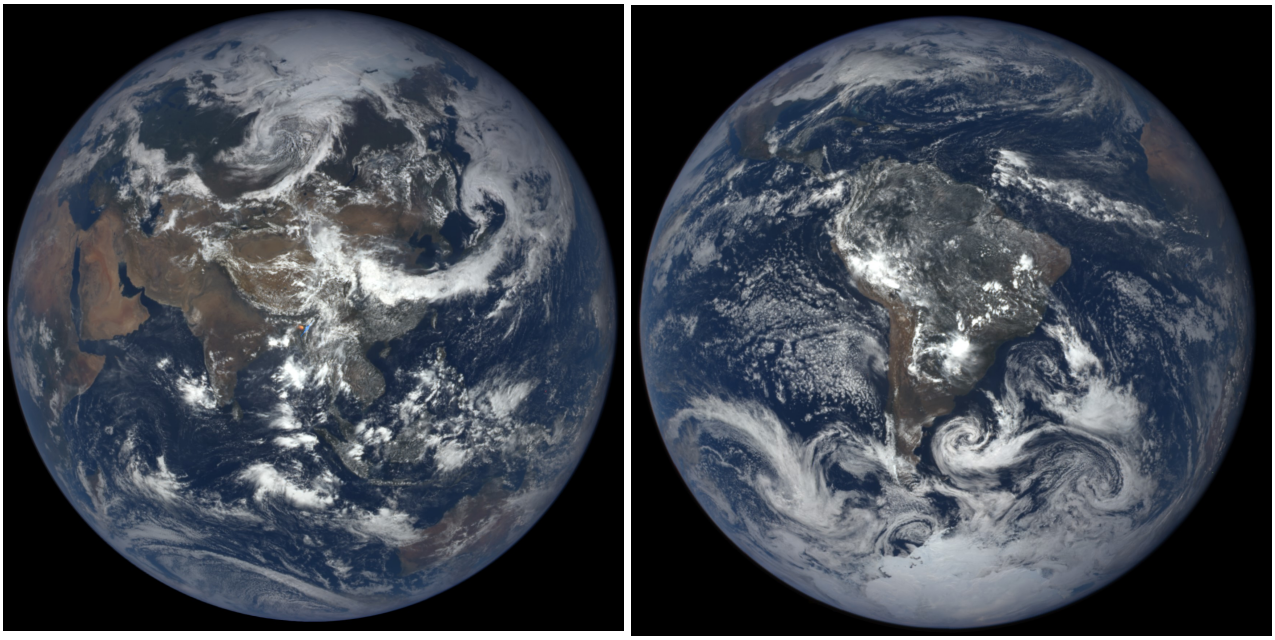

Figure 2-1 Natural Color EPIC Earth images from June 6 and December 6, 2016 showing the field of view during the respective hemispheric summers. In both of these images, 6-months apart, The EPIC orbit is to the west of the Earth-Sun line causing the west side of the globe (sunrise) to appear brighter than the east side (sunset). Notice the bright specular reflection over Argentina, South America embedded within a cloud feature. This is thought to be from ice crystals, which will be the subject of a separate paper.

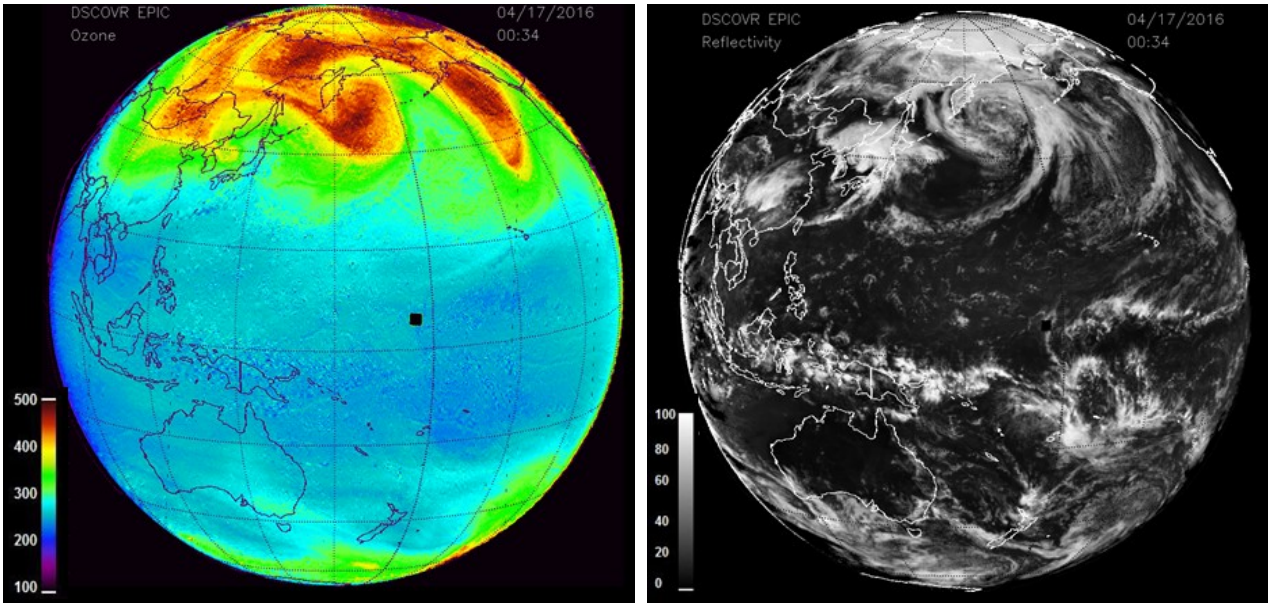

Figure 3-1 EPIC retrieved ozone and LER values for April 17, 2016. The ozone scale is from 100 to 500 DU, and the LER scale is from 0 to 100 percent.

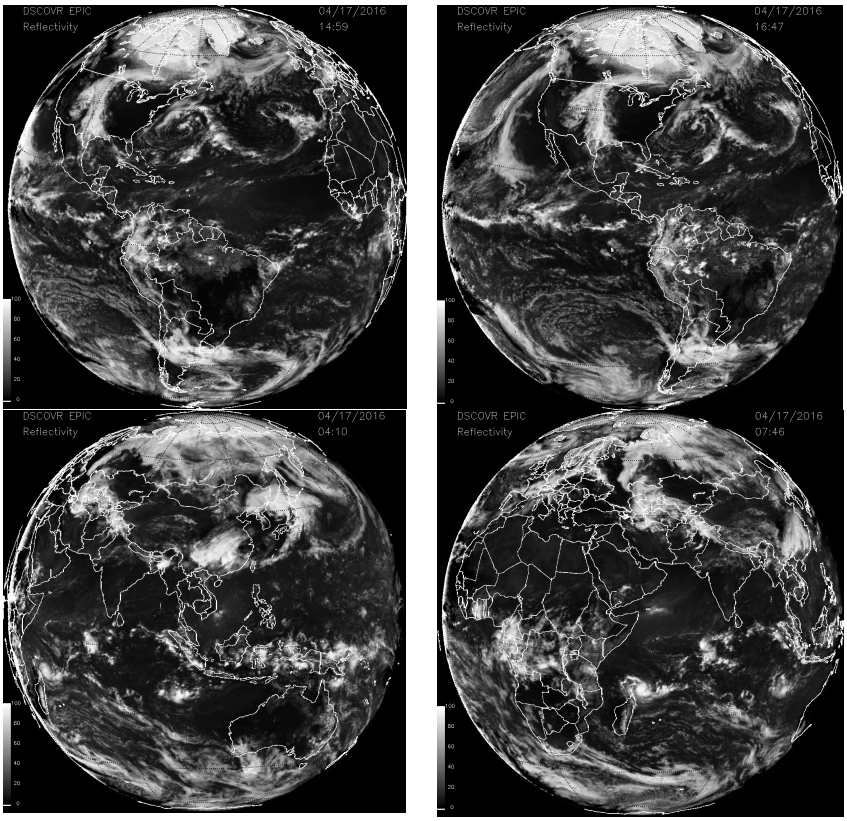

Figure 3-2 Cloud formations from 17 April 2016 showing the Arctic at 4 different GMT's, 14:50, 16:47, 04:10, and 07:46. The same scale as Figure 3-1 LER.

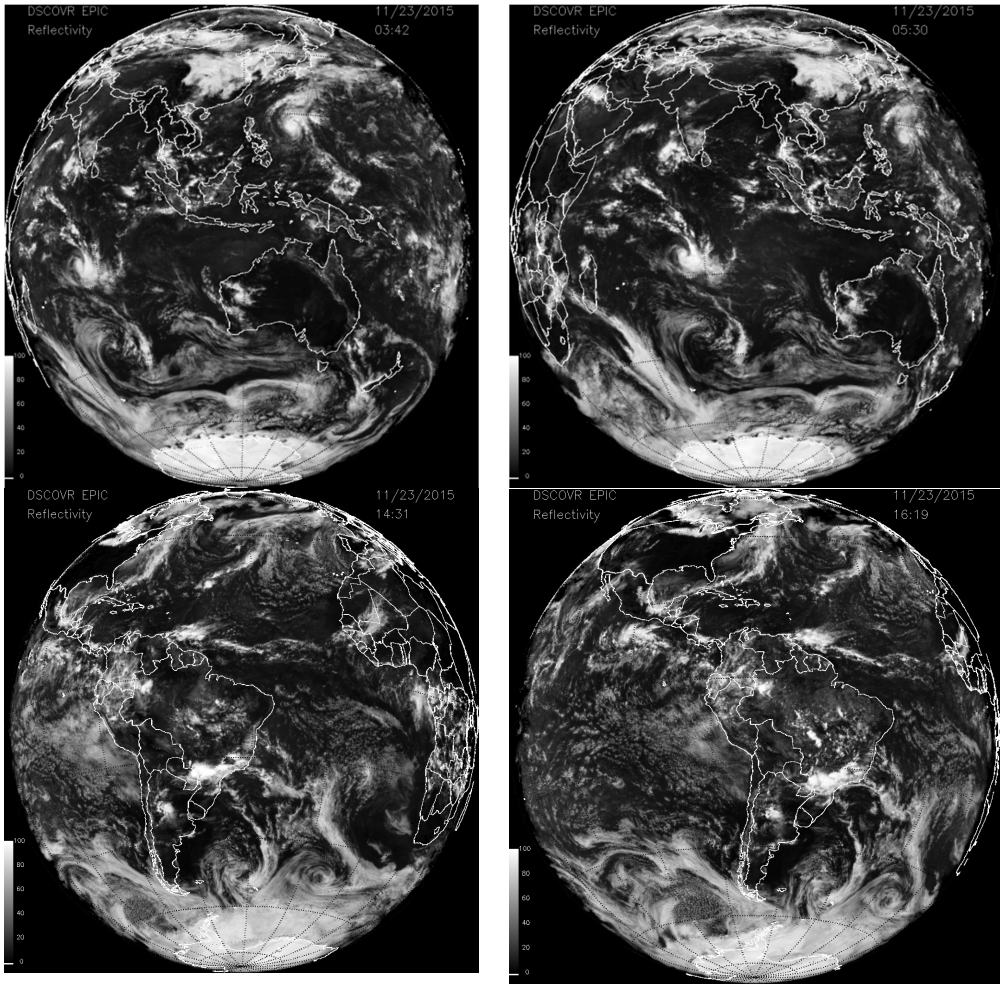

Figure 3-3 Cloud formations from 23 Nov 2015 showing Antarctica at 4 different GMT's, 03:42, 05:30 14:31, and 1619. The same scale as Figure 3-1 LER.

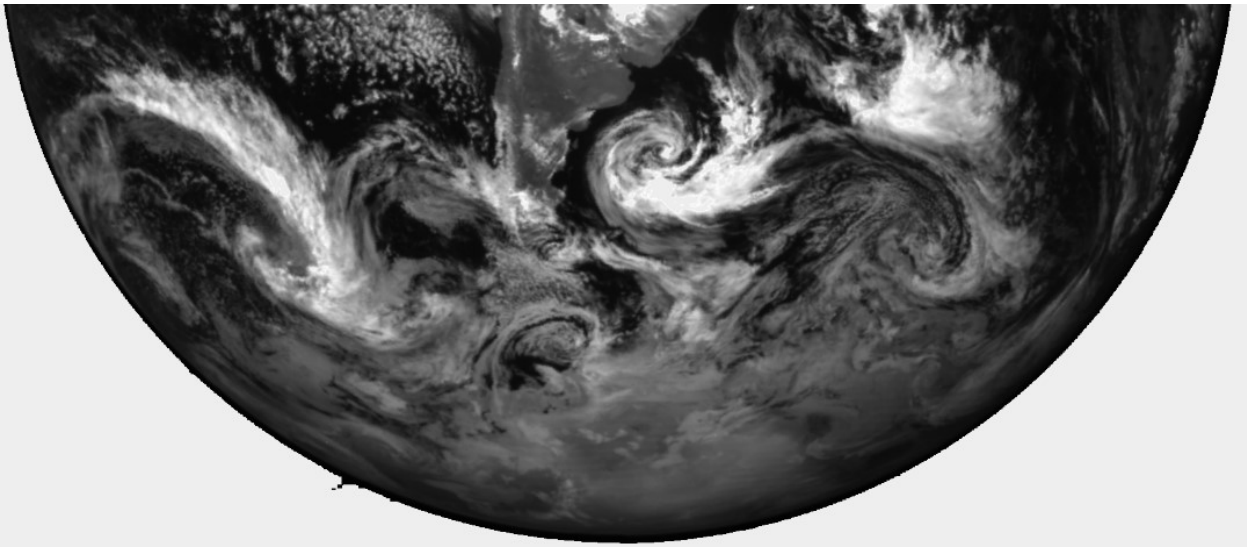

Figure 3-4 O_2 A-band View of Antarctica on December 6, 2016 showing clouds over ice. The white bright clouds are at higher altitudes than the dull grey clouds because of a combination of less absorption and higher optical depth.

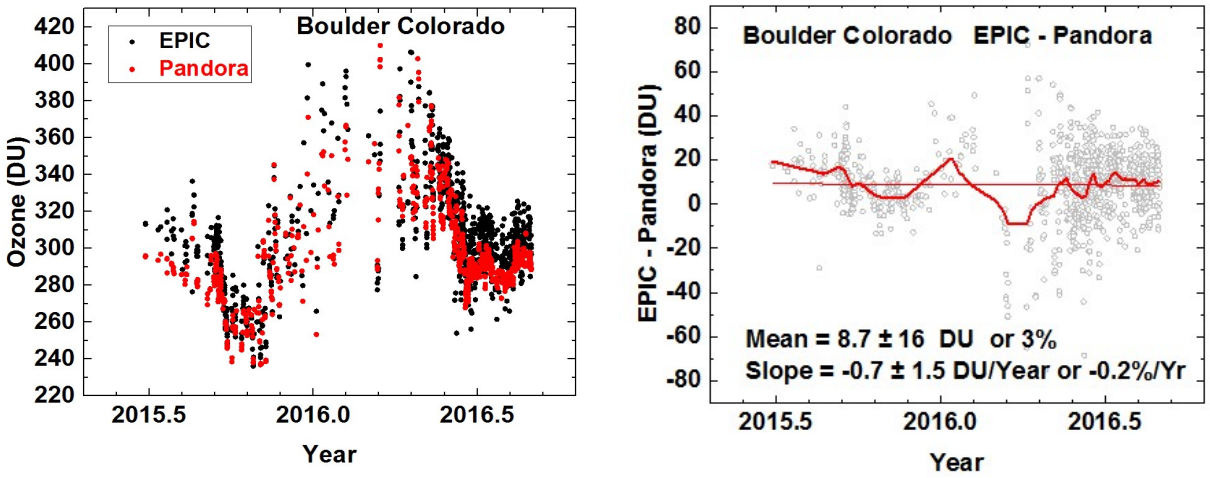

Figure 4-1 Left: EPIC ozone data compare to Pandora retrievals at Boulder Colorado. Right: Daily (grey circles) and Monthly (red line) average difference between Pandora and EPIC ozone retrievals.

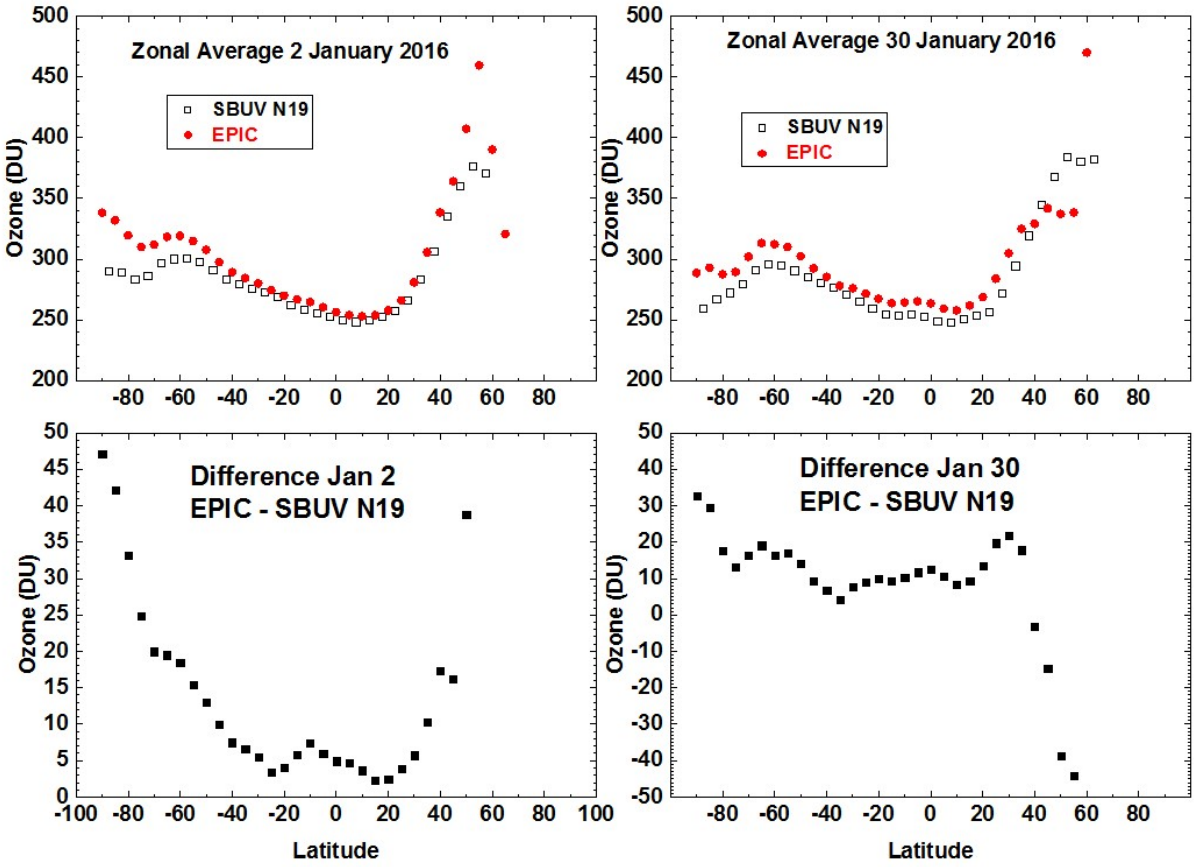

Figure 4-2 A comparison of zonal average ozone between EPIC and NOAA-19 SBUV satellite zonal averages

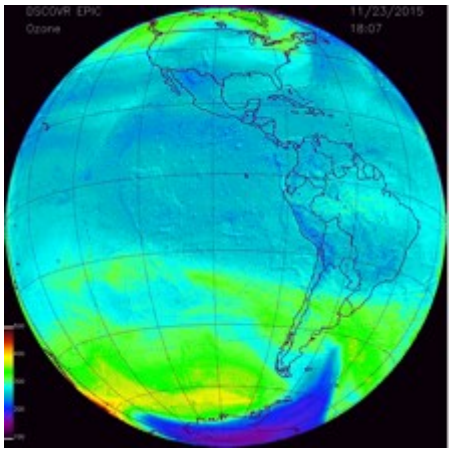

Figure 5-1 Global image of ozone field for Figures 5-2 and 5-3 for 23 Nov 2015 at 18:07 GMT

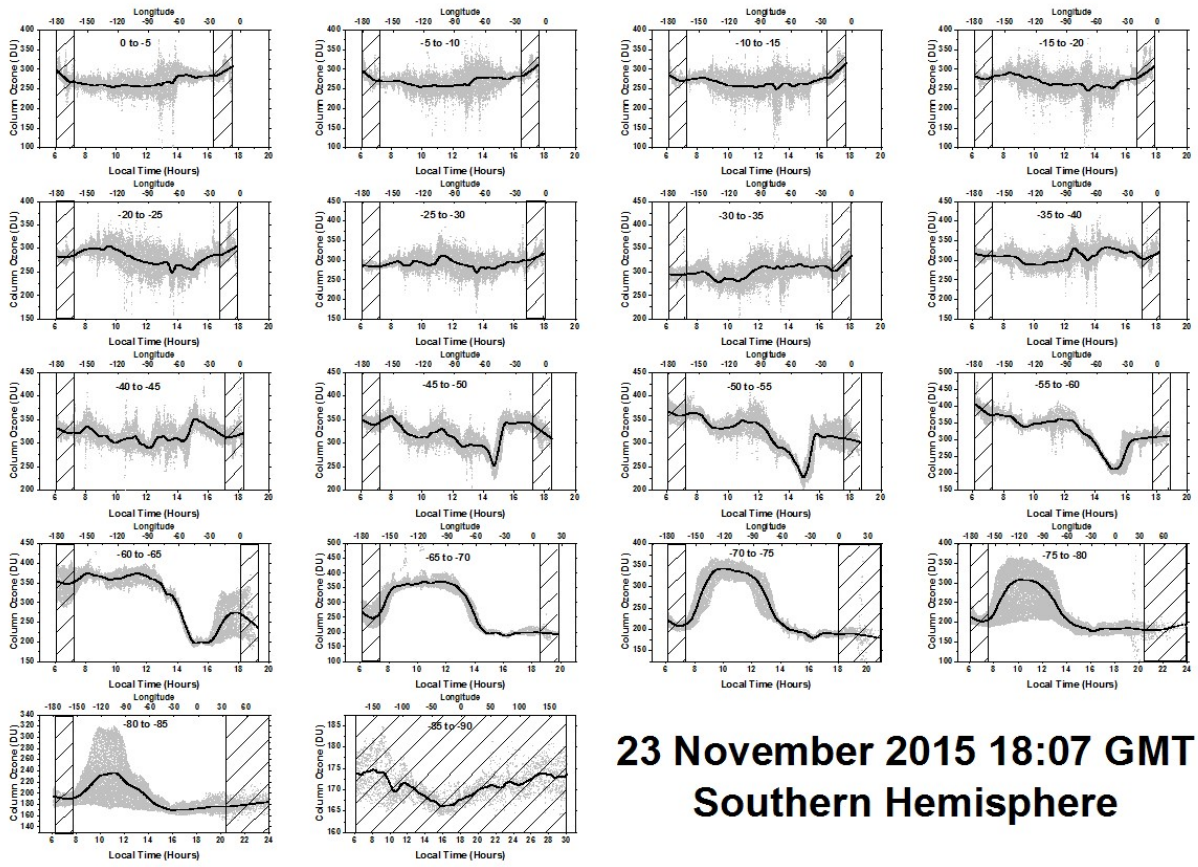

Figure 5-2 Diurnal variation of ozone for the Southern Hemisphere every 5^{O} degrees from 0^{O} to $90S^{O}$ for 23 Nov 2015 at 18:07 GMT. The grey bands are the individual data points in the band. The solid lines are a Lowess(0.05) fit to the data points representing a solar time average from 0.6 to 0.7 hours depending on latitude. The cross-hatched lines are a rough estimate of where the SZA or SLA might be too large for accurate ozone retrieval.

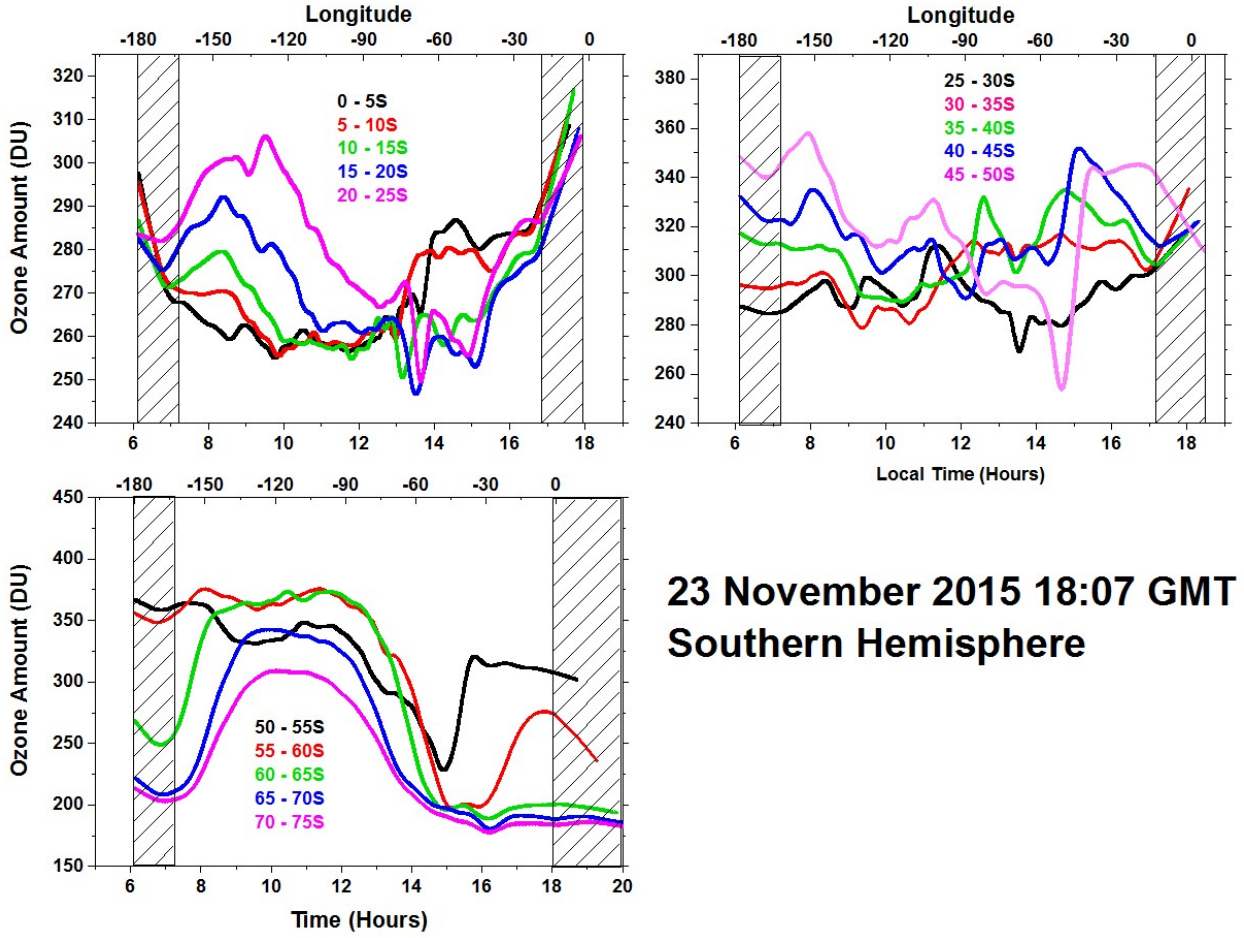

Figure 5-3 Approximately 30 minute averages in solar time at 18:07 GMT on 23 November 2015 for ozone variation between 0^{O} and 75^{O}S latitude in 5^{O} latitude bands.

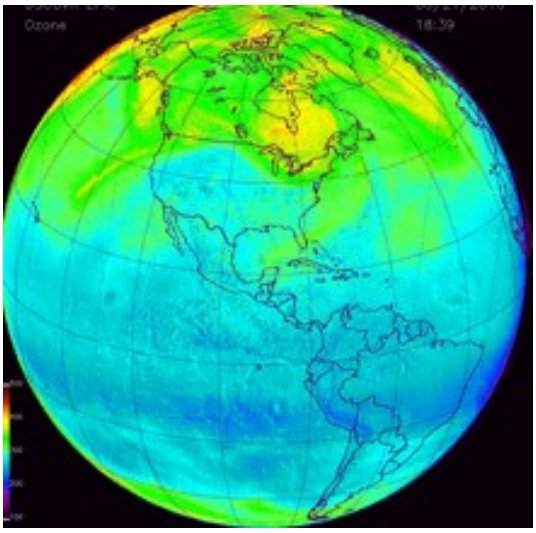

Figure 4-4 Global image of ozone field for Figures 4-5 and 4-6 for 21 June 2016 at 18:39 GMT

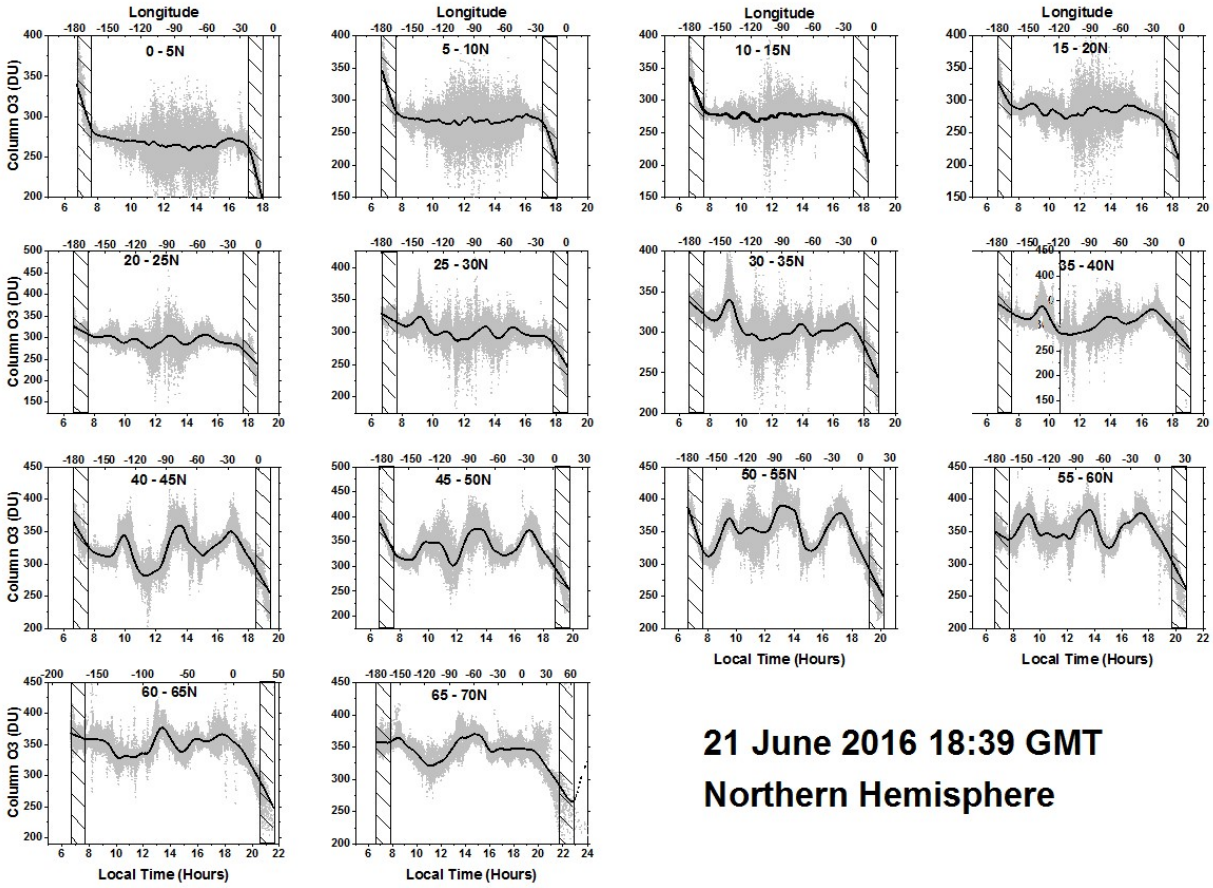

Figure 4-5 Diurnal variation of ozone for the Northern Hemisphere every 5^{O} from 0^{O} to 70^{O} for 21 June 2016 at 18:39 GMT. The grey bands are the individual data points in the band. The solid lines are a Lowess(0.05) fit to the data points representing a solar time average from 0.6 to 0.7 hours depending on latitude. The cross-hatched lines are a rough estimate of where the SZA or SLA might be too large for accurate ozone retrieval.

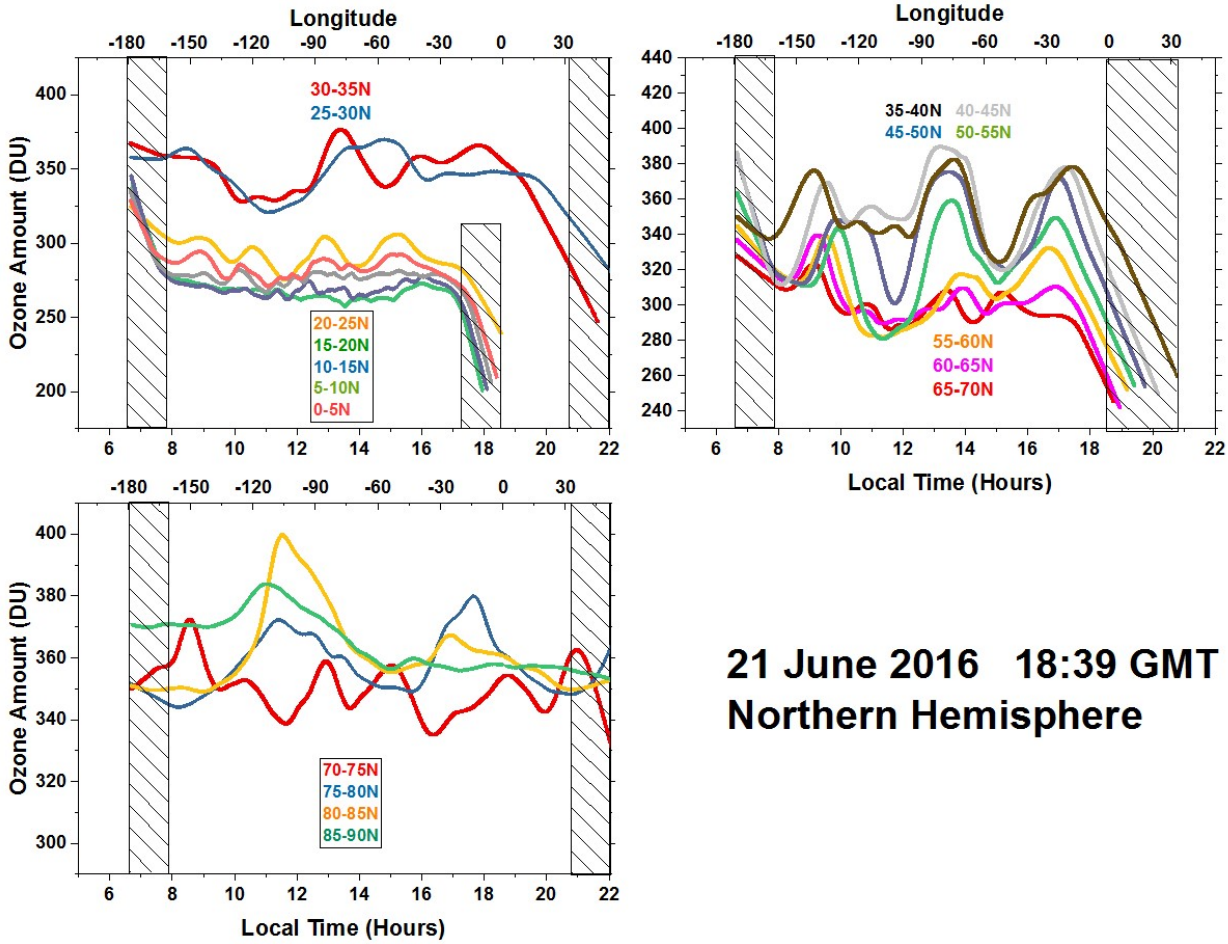

Figure 4-6 Approximately 30 minute averages in solar time at 18:39 GMT on 21 June 2016 for low latitude ozone variation between 0^{O} and 35^{O}N, 35^{O} to 70^{O} N, and 70^{O}N to 90^{O}N in 5^{O} latitude bands.

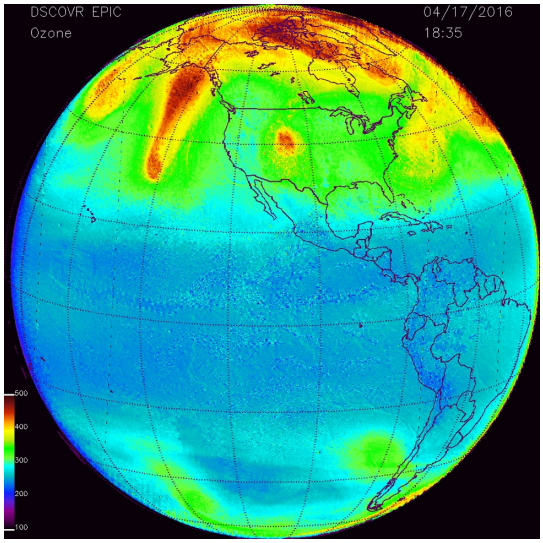

Figure 4-7 Global image of ozone field for Figure 4-8 for 17 April 2016 at 18:35 GMT

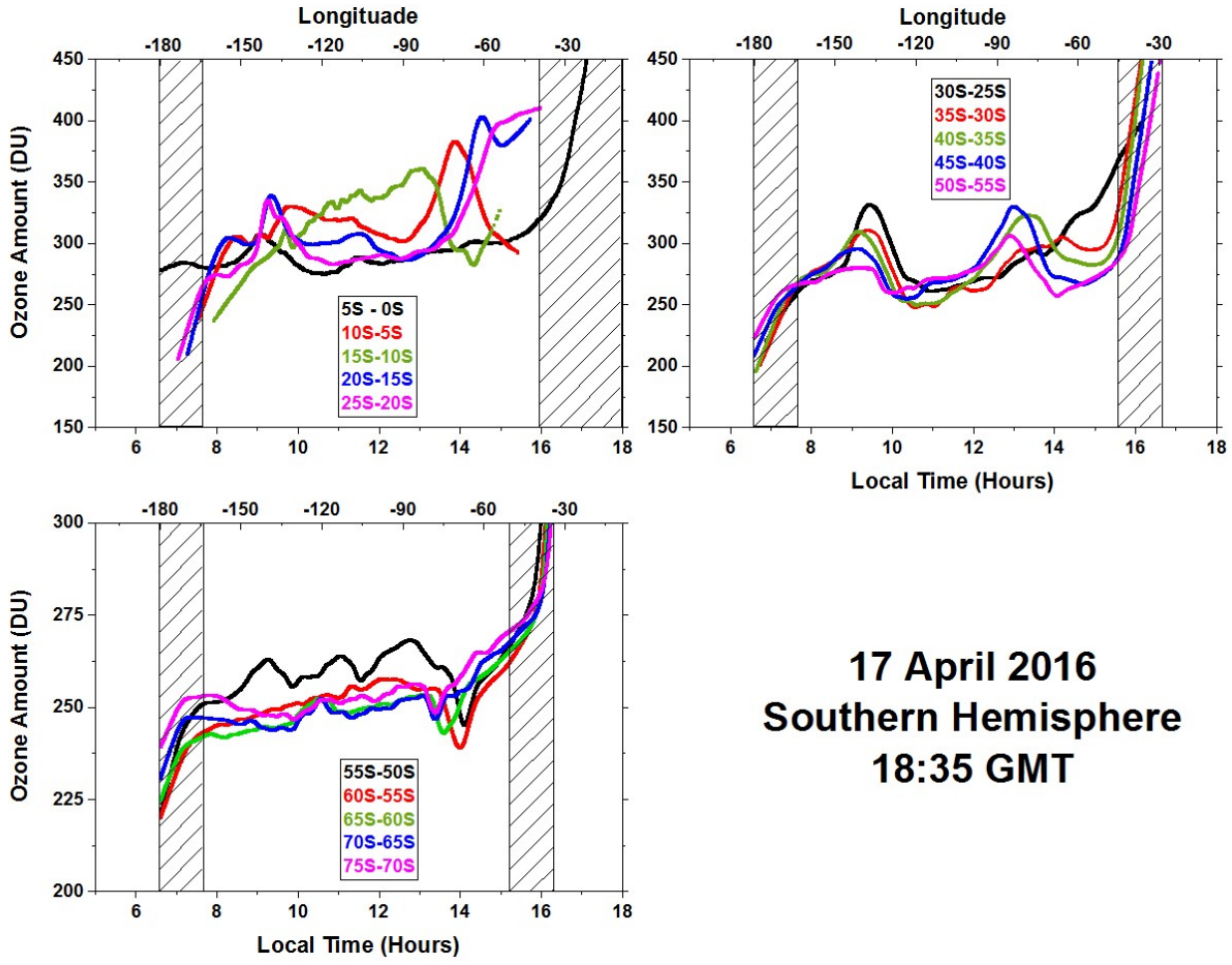

Figure 4-8 Approximately 30 minute averages in solar time at 18:35 GMT on 17 April 2016 for ozone variation between 0^{O} and 75^{O}S latitude in 5^{O} latitude bands.

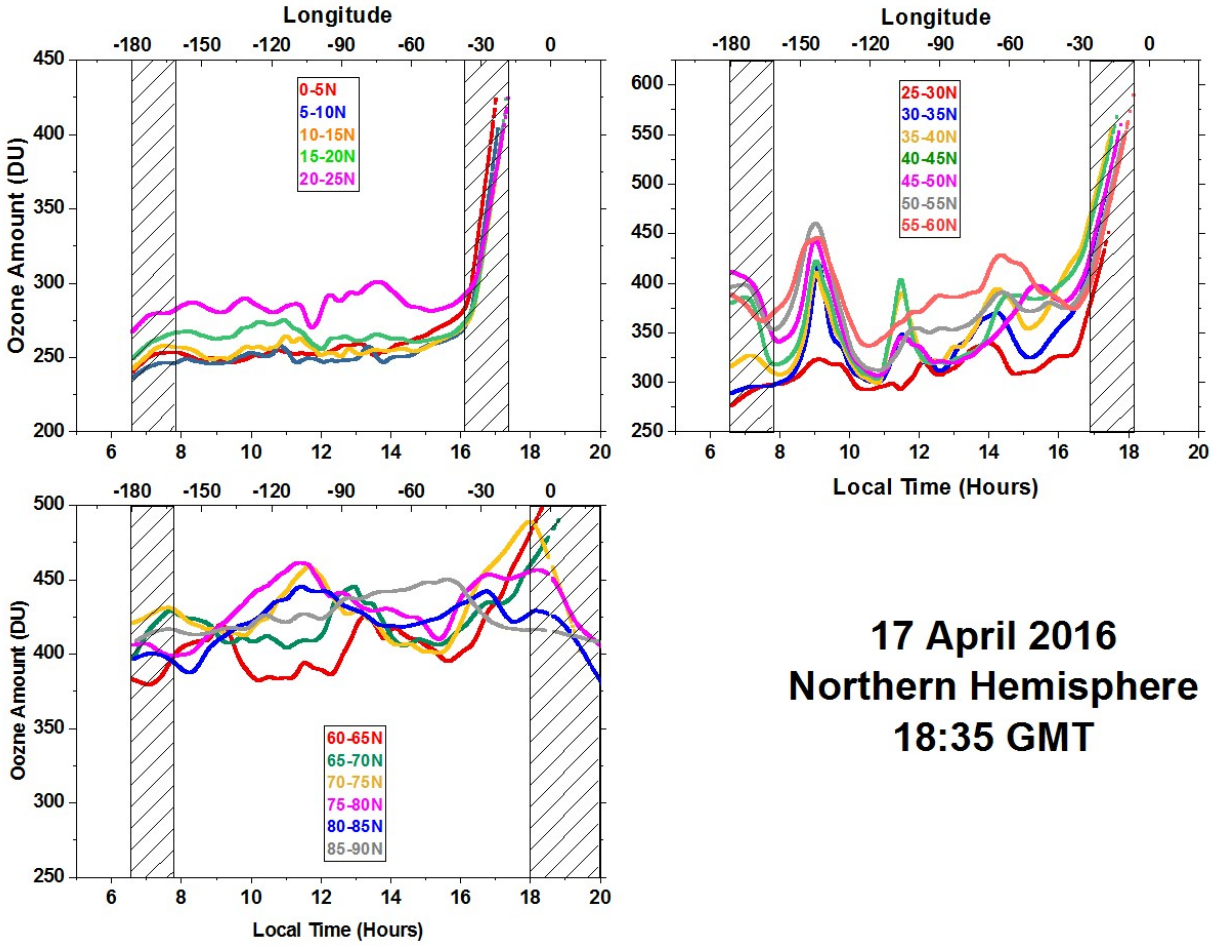

Figure 4-9 Approximately 30 minute averages in solar time at 18:35 GMT on 17 April 2016 for ozone variation between 0^{O} and 90^{O}N latitude in 5^{O} latitude bands.

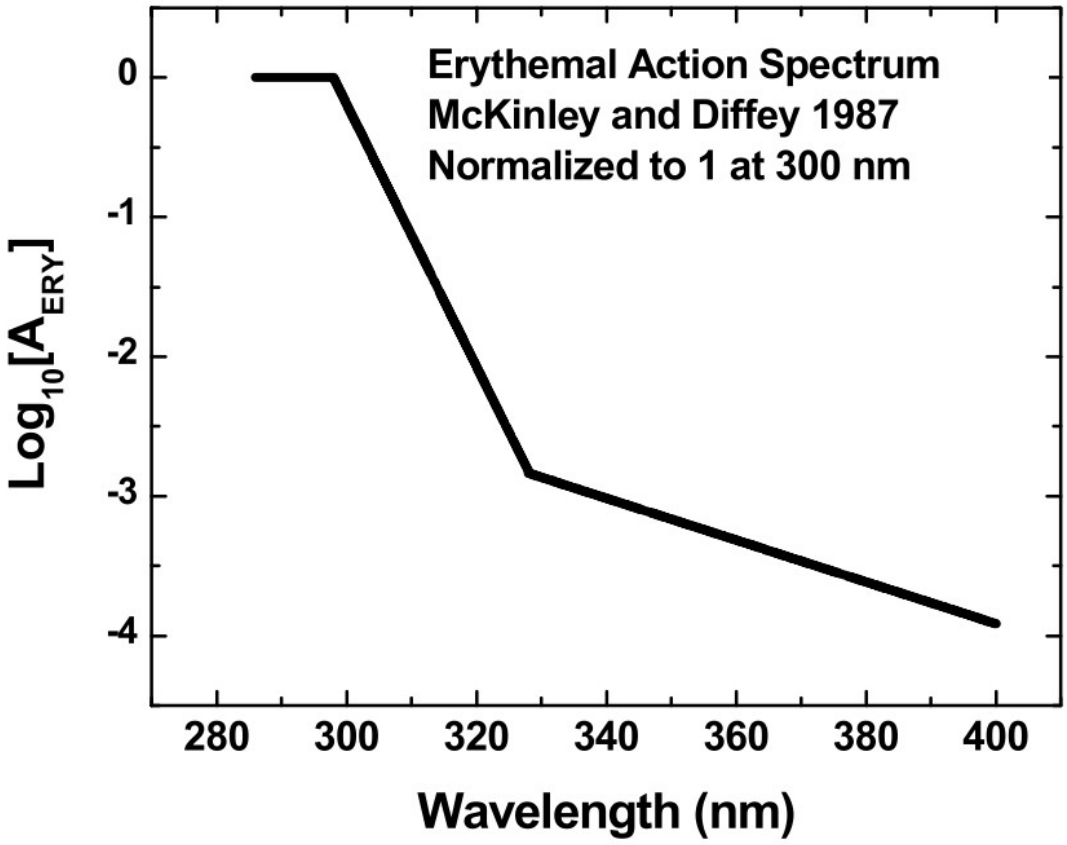

Figure 5-1 $Log_{10}(A_{ERY})$ where AERY is the Erythemal action spectrum.

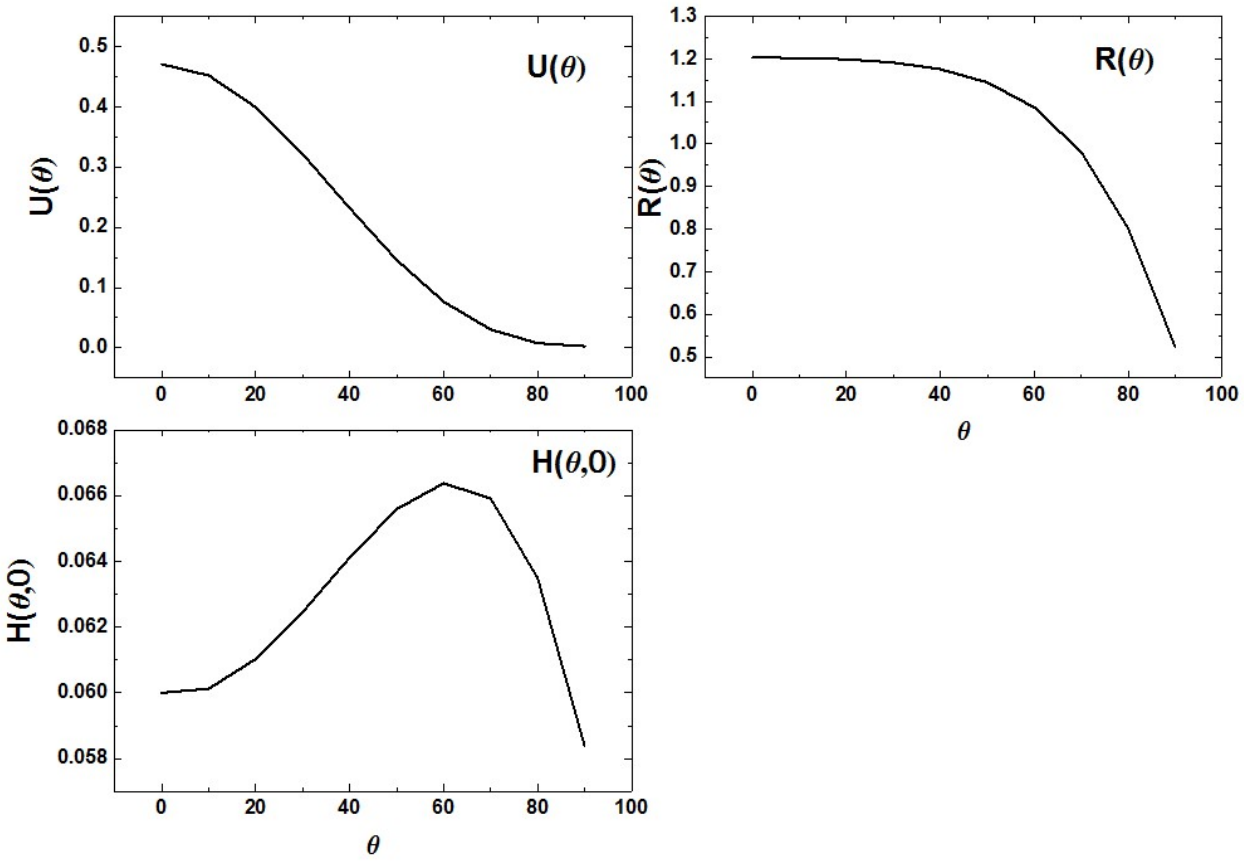

Figure 5-2 Coefficients for the Erythemal fitting function

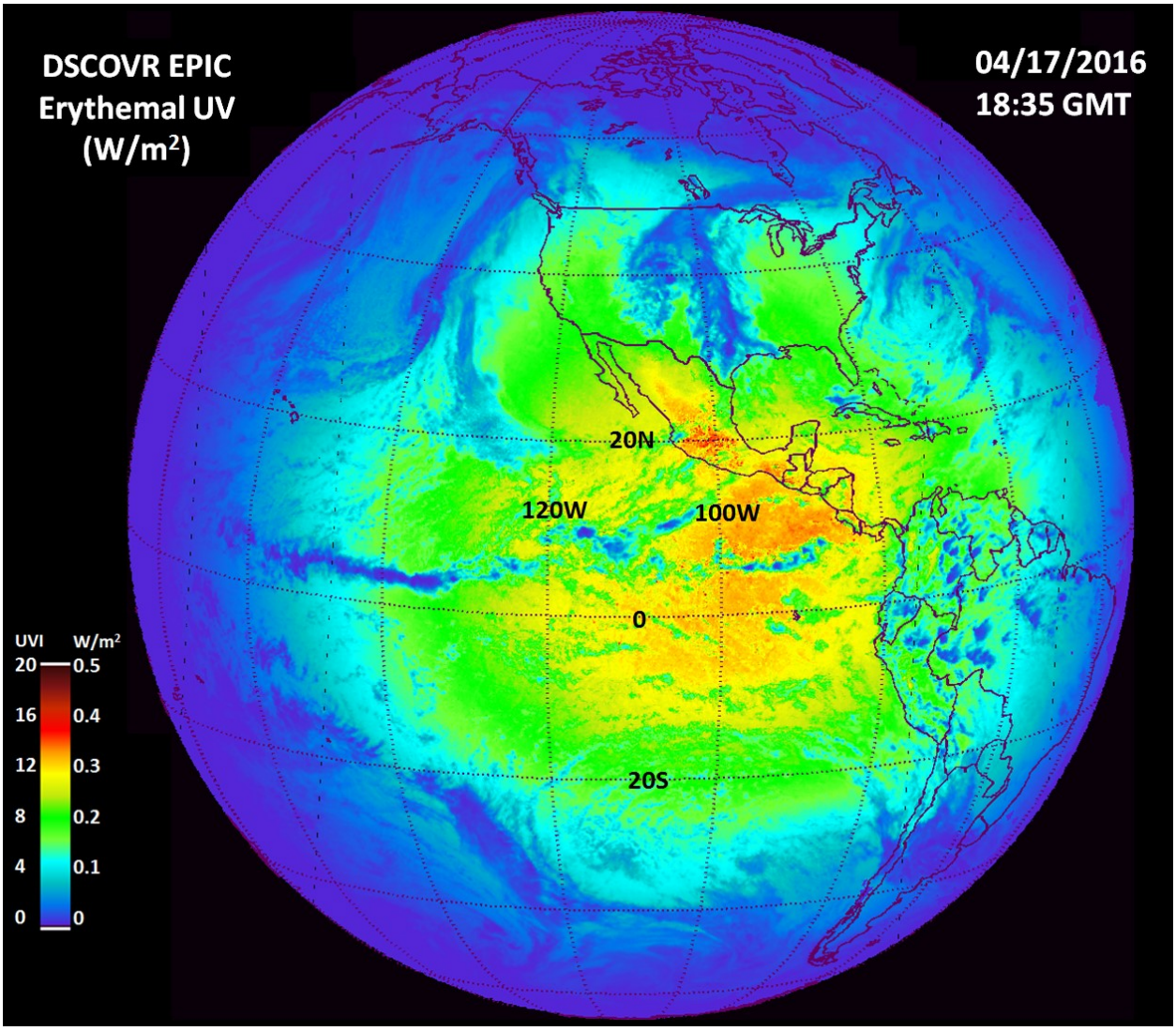

Figure 5-3 Erythemal irradiance calculated from Equation 4-3 and from the EPIC ozone and LER data obtained on April 17, 2016 at 18:35 GMT. The scale shows both the irradiance values in W/m2 and the UV index ranging from 0 to 20. This scene is centered over the Pacific Ocean and shows a peak UV index of about 15. Since this period is close to equinox, the sun is nearly overhead just north of the equator with solar noon at 98.75W longitude and overhead near 10N.

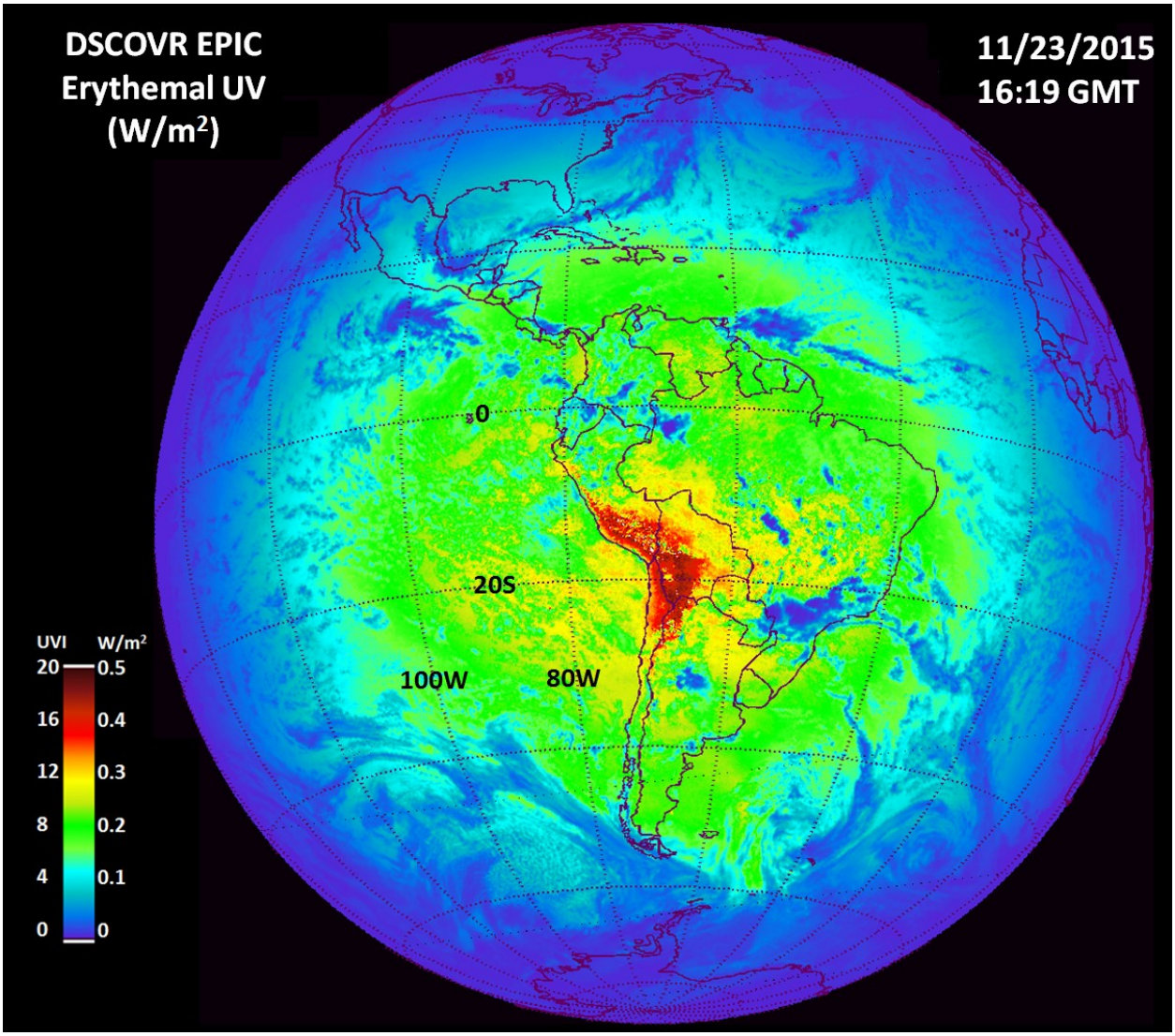

Figure 5-4 Erythemal irradiance centered over South America on November 23, 2015 at 16:19 GMT showing extremely high values in the Andes Mountains in Peru and Chile corresponding to a UV index greater than 20. Local solar noon is at 64.75W and overhead near 20S.

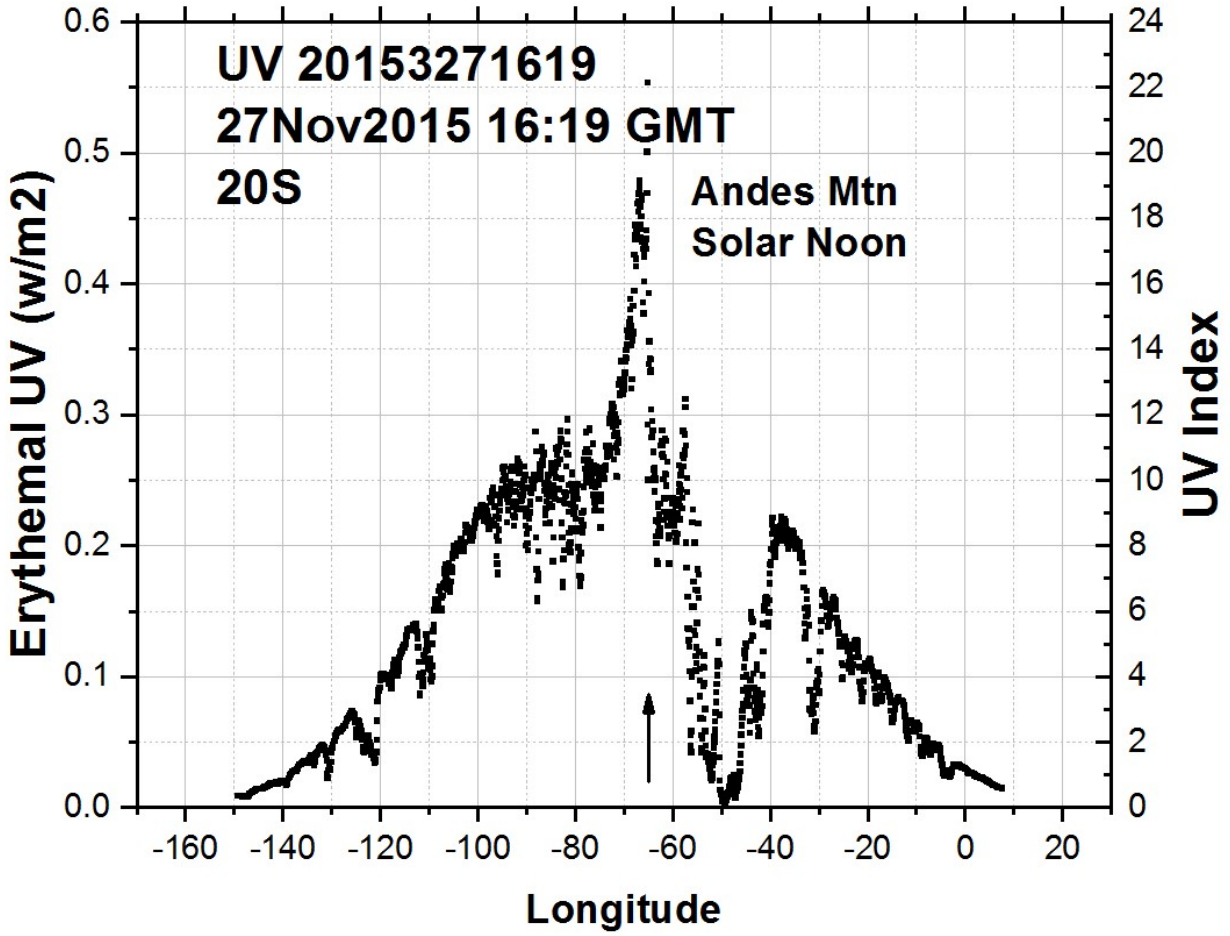

Figure 5-5 Erythemal Irradiance in a longitudinal slice at 20S through a peak occurring in the Andes mountains. Local noon is at 64.75W.

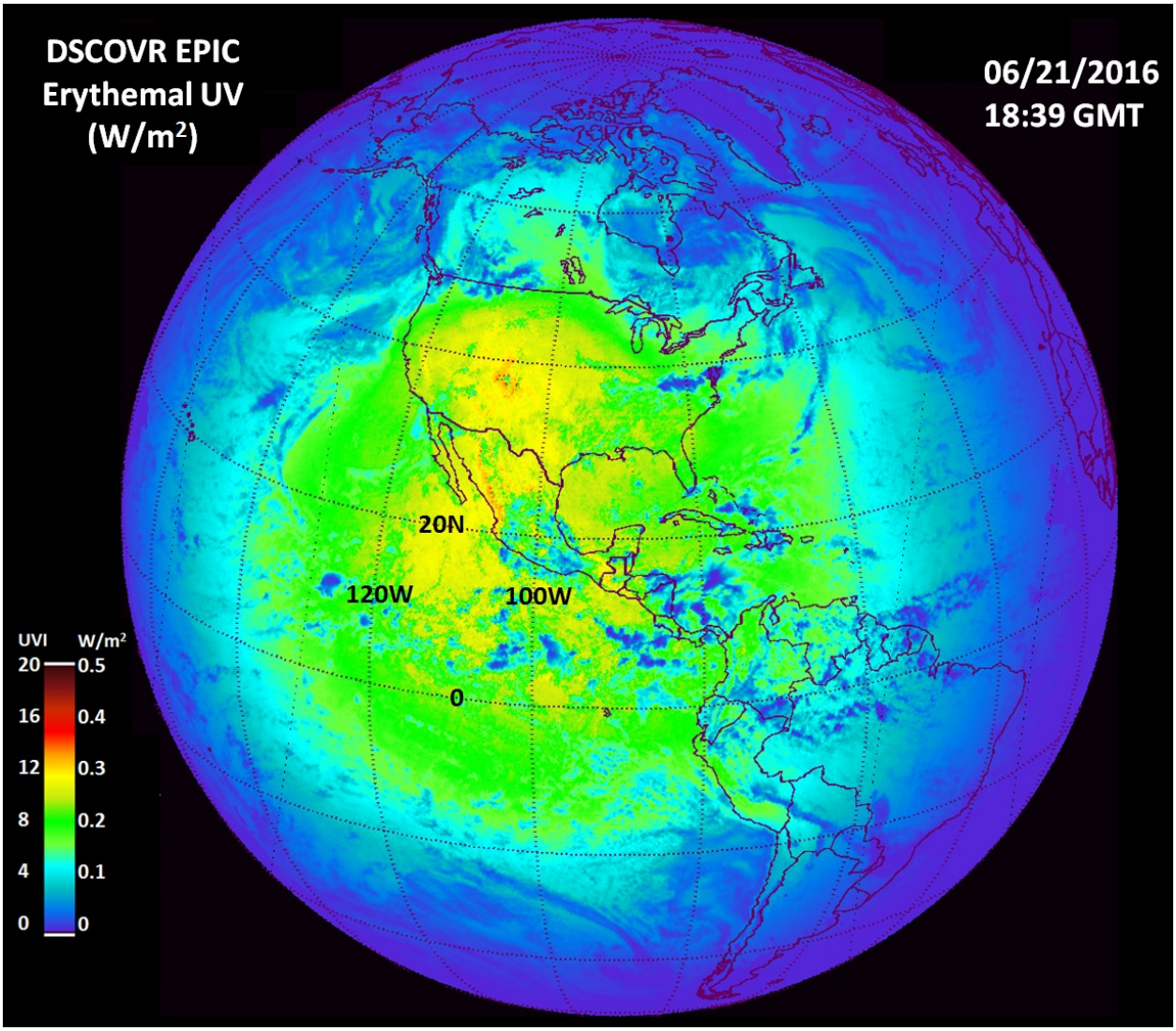

Figure 5-5 Erythemal irradiance centered over the United States on June 21, 2016 showing high values over the Rocky Mountains and a portions of the Sierra Nevada Mountains. The UV index reaches about 15. Local solar noon is at 99.75W and overhead near 23.3N.

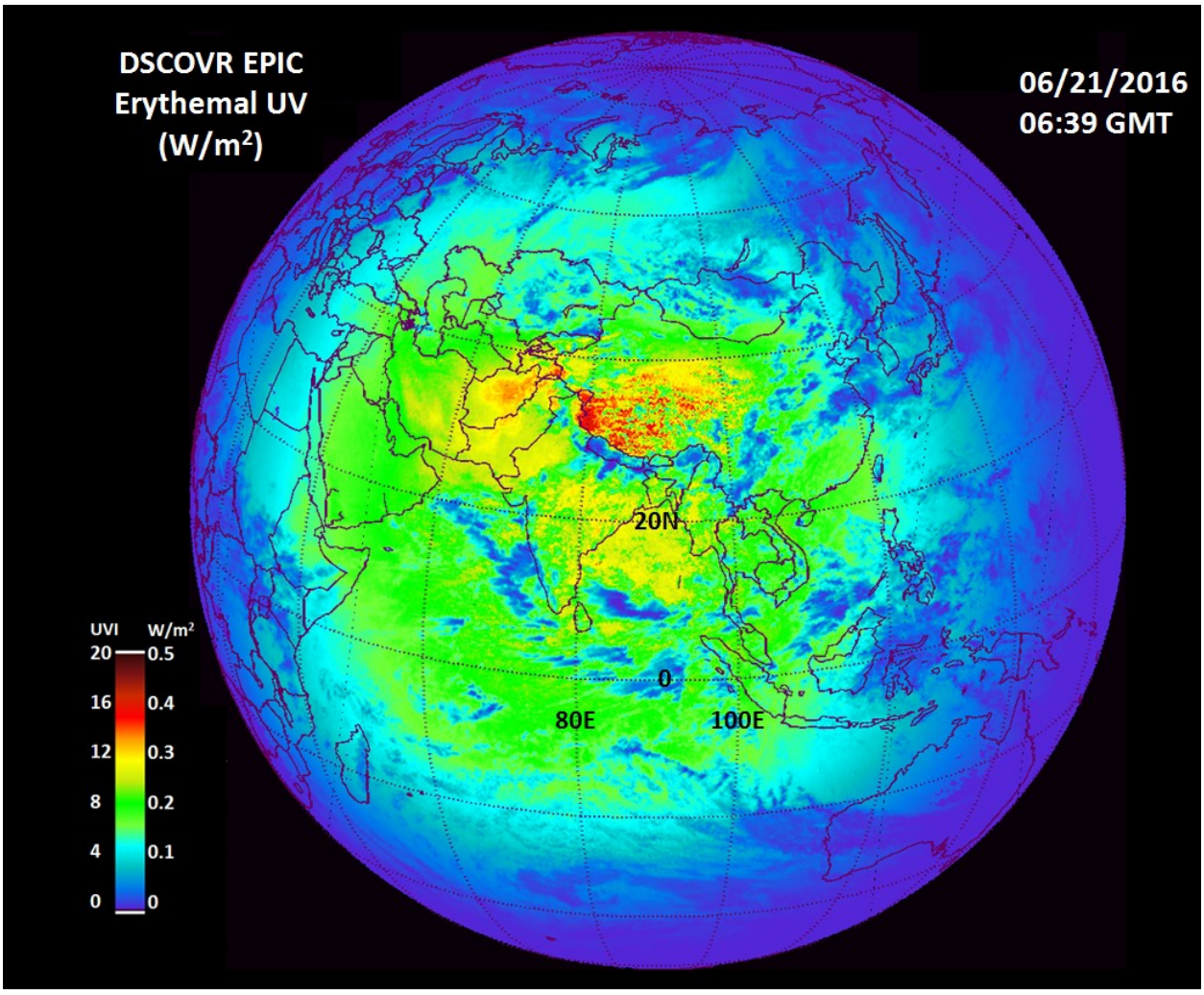

Figure 5-6 Erythemal UV irradiance centered over the Indian Ocean on June 21, 2016 showing high values over the Himalayan Mountains with the UV index exceeding 14. UV levels are moderated by partial cloud cover reflection of radiation back to space. Solar noon is at 80.25E

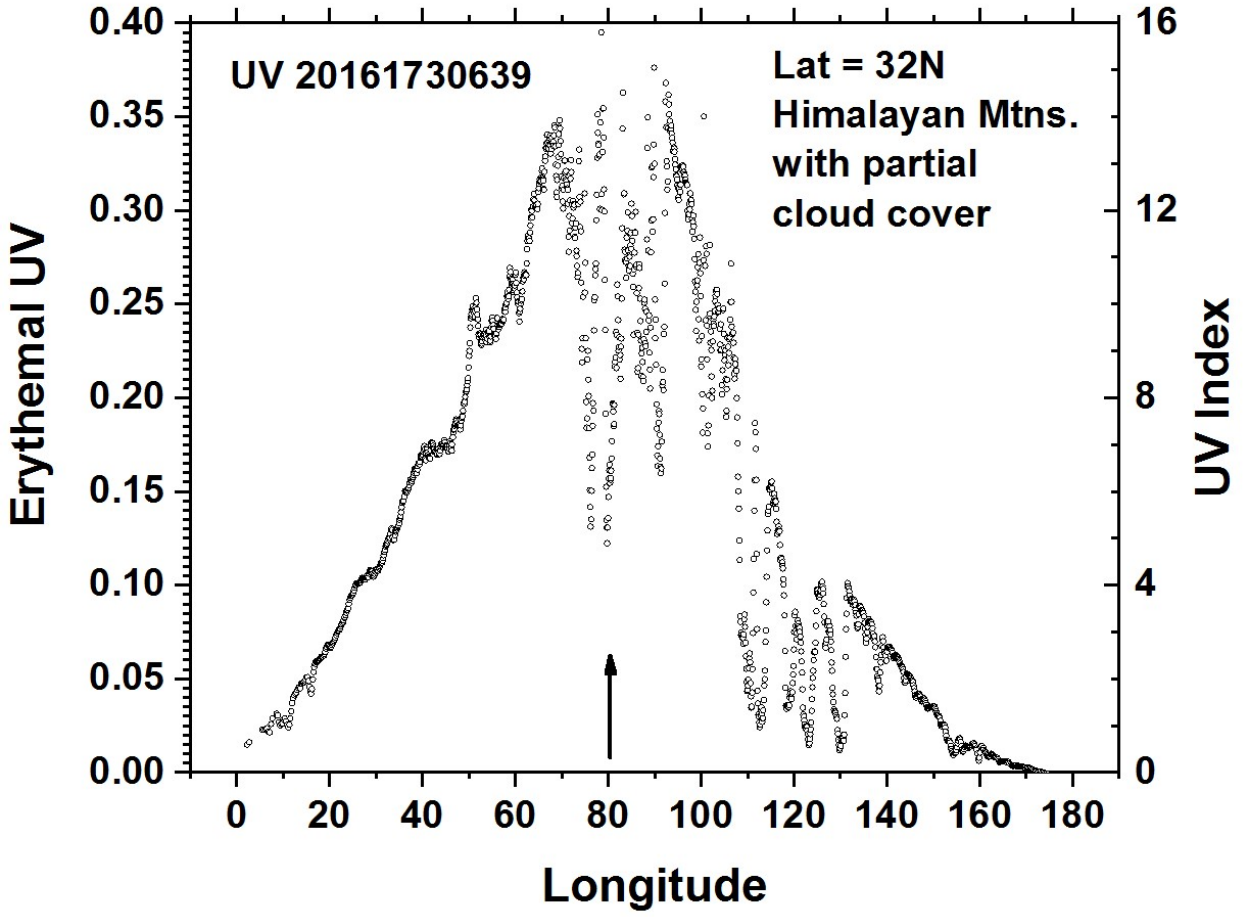

Figure 5-7 Erythemal Irradiance in a longitudinal slice at 32N through a portion of the Himalayan mountains. Local solar noon is at 80.25E.